ISBN: 978-3-95450-220-2 ISSN: 2673-5474 doi: 10.18429/JACoW-FEL2022-WEAO4

CHIRPED PULSE LASER SHAPING FOR HIGH BRIGHTNESS PHOTOINJECTORS

C. Koschitzki, H. Qian, Z. Aboulbanine, G. Adhikari, N. Aftab, P. Boonpornprasert, G. Georgiev, J.D. Good, M. Gross, A. Hoffmann, M. Krasilnikov, X. Li, O. Lishilin, A. Lueangaramwong, G. Loisch, R. Niemczyk, A. Oppelt, G. Vashchenko, T. Weilbach, F. Stephan, DESY Zeuthen, Germany
I. Hartl, DESY Hamburg, Germany

Abstract

In this publication we show the current status on spectral-spatial shaping at the Photo Injector Test Facility at DESY in Zeuthen (PITZ). The laser pulse shaper presented here is based on spectral amplitude modulation of chirped laser pulses. In this unique approach one can modulate the spatial profile of individual time slices in density and diameter. The photoinjector requires a wavelength of 257.5 nm, but the laser shaping applies at a wavelength at least greater than 400 nm, in this paper, at 1030 nm. Both the shape preservation and fourth harmonic generation efficiency of the chirped laser pulses are discussed.

INTRODUCTION

The free electron laser (FEL) is currently the most powerful source for coherent X-rays. It is typically based on linear electron accelerators, which rely on a low transverse emittance electron source, to allow X-ray lasing in the undulator. As the emittance in modern FELs is limited by the source emittance, it is intuitive to also optimize the photoemission laser shape to control the emittance growth due to nonlinear space charge forces during the low energy transportation. For electron beams, dominated by space charge effects, it was shown that shaping of the extracting laser pulse can reduce the space charge induced emittance growth [1] [2]. Another study shows, that slice mismatch of a triangular driver beam for high efficiency beam based plasma acceleration can be reduced [3], if the extraction laser allows for independent control of slice charge and charge density. A Spatial Light Modulator (SLM) based laser pulse shaper with such a capability has been proposed by Mironov [4] and a variation of such a shaper has been used to shape the output of an infrared (IR) laser amplifier at 1030 nm. The photo injector cathode requires a UV pulse to extract electrons, thus the fourth harmonic was obtained from two consecutive second harmonic generation (SHG) stages. A high quality laser pulse shaping was demonstrated for the IR pulses.

SLM SHAPER

The shaper is an imaging zero compressor or Martinez system as shown in Fig. 1, where a 4f-telescope with two identical lenses images the surface of one grating to another grating and ultimately path length differences of different wavelengths add up to zero. The SLM is then placed at the Fourier plane in between the two lenses, where a collimated

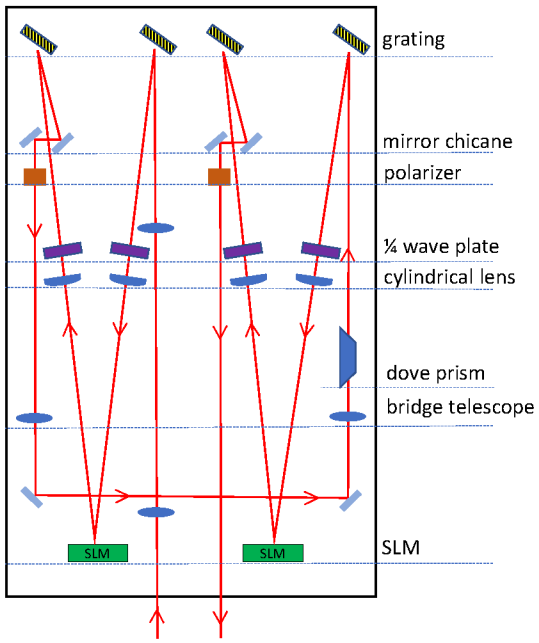

Figure 1: Schematic of a double SLM Shaper.

beam in absence of the gratings would be focused. Due to the grating dispersion the intensity distribution at the SLM plane parallel to the table corresponds to the spectral amplitude distribution. This is still true, if cylindrical lenses are used and the lens rotation is aligned with the grating rotation. But since neither the grating nor the lenses act on the transverse vertical axis, the optical transfer is identical to a free drift for the transverse vertical axis. Thus in the vertical plane an image of the SLM can be transported, if the lens is placed outside the shaper, i.e. after the second grating. Then of the two axis of our two dimensional SLM, one axis corresponds to spectrum, while the other corresponds to a spatial axis like in a typical spectrograph setup. The liquid crystals in an SLM act as polarization dependent phase shifters and a setup like this could be operated as a digital prism. In order to turn it into an attenuator we can use two quarter wave plates at 45 degrees, before and after the SLM. This turns the phase shift into a polarization rotation and thus 180 degrees of phase shift become an attenuation between 0 and 100% after a subsequent polarizer. As only one spatial dimension is accessible in a single shaper, the laser beam is rotated by 90 degree using a Dove Prism and sent through a

ISBN: 978-3-95450-220-2 ISSN: 2673-5474 doi: 10.18429/JACoW-FEL2022-WEAO4

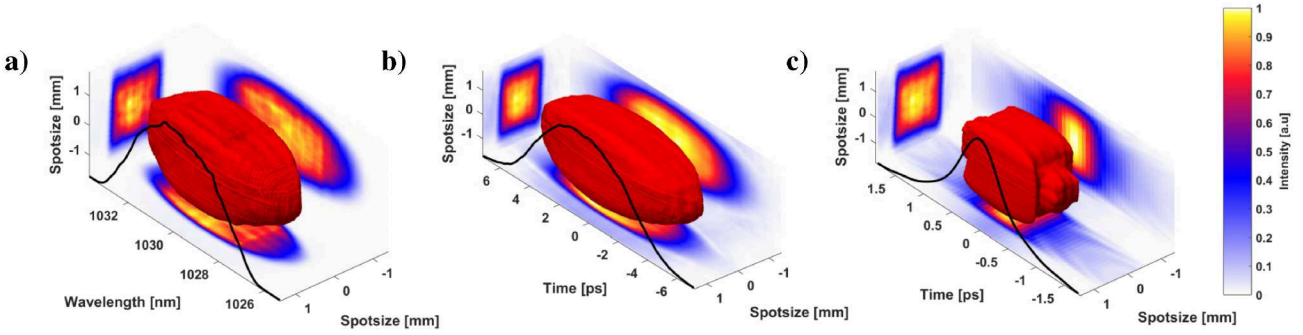

Figure 2: Volume data of spectrograph slitscan with isosurface 25% peak intensity and projections for **a)** the spectrograph data and for Eq. (2) applied to longitudinal axis with group velocity dispersion (GVD) of **b)** 0.8 ps^2 and **c)** 0.1 ps^2 respectively.

second identical shaper setup. The bridge part between the shapers needs to take into account that the image of the first shaper is propagated in the second shaper and the images have separated image planes. Our optical simulations have shown that one solution is to image output grating to input grating with a 4f-telescope with magnification of one and a focal length longer than the focal length of the cylindrical lens inside the shaper. The attenuation of a single shaper is a function of the form $f_a(x, \lambda)$ which can be applied to the initial laser intensity distribution $I(x, y, \lambda)$, typically a 3D gaussian. The final attenuation function can be written as:

$$f_a(x, y, \lambda) = f_{a1}(x, \lambda) \cdot f_{a2}(y, \lambda), \quad (1)$$

which can not be rotationally symmetric in the x-y plane, because of the missing x-y correlation. A third transverse SLM shaper was added to the setup with $f_{a3}(x, y)$, but has no distinction in the wavelength domain. Thus a 3D radial symmetry around the propagation axis can still not be achieved. Figure 2 shows a measurement of a shaped quasi ellipsoid. It was obtained using a volume slit scan with a spectrograph. The spatial-temporal laser pulse profile can then be obtained by a Fourier transformation including the spectral phase.

$$I(x, y, t) = Fourier(I(x, y, \lambda) \cdot e^{i*GDD^2*\lambda^2})d\lambda. \quad (2)$$

The GVD is obtained from the geometric parameters of the compressor in our chirped pulse amplifier (CPA) system. Our CPA system provides laser pulses with a 7 nm FWHM spectra and a transform limited pulse duration of 300 fs FWHM. Our target pulse duration is between 10-20 ps with a typical group delay dispersion of 1.5 ps^2. At these large GVD the distributions in Eq. (2) become self similar.

With laser pulses significantly closer to the transform limit, the required spectral distribution for most desired temporal pulse shapes might not be achievable, given the symmetry condition by Eq. (1). Some distributions might theoretically be achievable, but with low shaping efficiency ε_s. It is calculated by the best fit of the desired spectral-spatial distribution under the initial distribution. Also more complex spectral phase distributions are achievable and temporal shapers exist, that rely fully on spectral phase shaping [5].

CONVERSION

The shaped IR pulses have to be converted to UV wavelength and conversion efficiency has to be weighed against pulse preservation considerations. In order to preserve the transverse shape, the nonlinear crystals have to be put in an image plane of our beam transport. Then the transverse output intensity distribution becomes approximately the square of the input distribution. A nonlinear conversion outside an image plane yields the square of the diffracted intensity and subsequently a distorted distribution at the image plane. For the case of conversion at the focal plane, this effect is typically similar to a low pass Fourier filter as high spatial frequencies get suppressed due to their low amplitude. This effect can still cause distortion if the Rayleigh length d_R becomes smaller or equal to the crystal thickness. Furthermore we will refer to it as nonlinear depth of field (NDoF). Another effect concerning the transverse shape is the nonlinear walkoff, as the generated harmonic pulse propagates at an angle θ through the crystal with respect to the fundamental. This leads to a linear smearing or walk-off δ of the generated harmonic distribution by $\delta = \theta \cdot d_c$ with the crystal thickness d_c. The temporal walk-off can be neglected in our case. The phase matching is done by critical phase matching, where the birefringent crystal axis are geometrically aligned to match the index of refraction for the center wavelength of our spectrum. Neighboring wavelength are only quasi phase matched and thus a limited phase matching bandwidth exists, which gets smaller with increasing crystal thickness. For BBO of 1 mm thickness the FWHM phase matching bandwidth is 0.792 THz or 0.7 nm around 515 nm respectively and thus smaller than the initial spectral width of 1.5 THz. For 0.25 mm crystal thickness the bandwidth increases to 3.17 THz and it is tolerable to counteract it with the shaper. Thicker crystals require additional broadband phase matching [6]. For conversion efficiency we can obtain a simple scaling law for two consecutive SHG processes. We assume efficiency is low, neglect saturation, assume perfect broadband phase matching. Thus the output pulse energy E_{VIS} of a single SHG from 1030 nm (IR) to 515 nm (VIS) scales like

$$E_{VIS} \propto E_{IR}^2 \frac{1}{\tau_{IR}} \frac{1}{M^2} d_{LBO}^2 \quad (3)$$

ISBN: 978-3-95450-220-2 ISSN: 2673-5474 doi: 10.18429/JACoW-FEL2022-WEAO4

and from VIS to UV like

$$E_{UV} \propto E_{VIS}^2 \frac{1}{\tau_{VIS}} \frac{1}{M^2} d_{BBO}^2 \tag{4}$$

thus follows

$$E_{UV} \propto E_{IR}^4 \frac{1}{\tau^3} \frac{1}{M^6} d_{LBO}^4 d_{BBO}^2 \tag{5}$$

The IR pulse duration τ_{IR} may not be identical to the VIS or UV pulse duration due to nonlinear pulse shortening, but they are proportional. In the case of a flattop they are identical. Similarly the transverse size may decrease through conversion steps, but will be proportional to the initial size and thus the magnification M of our variable telescope between shaper and conversion. The image magnification between LBO plane and BBO plane was fixed to $M = 1$ as we used 2 aspheric lenses with 50 mm diameter and 100 mm focal length, to maximize optical resolution. Lastly we approximated the dependency of the crystal thicknesses d_{LBO} and d_{BBO} to $\propto d^2$ for thin crystals. Thus we see that the transverse size has the biggest impact and should be set as low as crystal damage threshold and diffraction limited optical resolution allow, with a given pulse energy and duration. LBO thickness should be chosen to achieve approximately 50% conversion efficiency, which is slightly saturated. If for a given pulse duration and input IR pulse energy the UV pulse energy exceeds the requirements, the most promising trade is to decrease the BBO thickness, as it also has the larger nonlinear walkoff angle (85 mrad) and smaller phase matching bandwidth compared to LBO. Minimum BBO crystal thickness available was 100 µm. In Fig. 3 a transverse mask in the shape of the letter Pi was applied to the laser and the image was taken at each conversion step from IR to VIS to UV and eventually to electrons. The UV image on the PITZ cathode generated an electron distribution, which could be imaged to a fluorescent screen with magneto optical transport. The transverse shape was reasonably preserved in this scenario, but conversion efficiency was very low and only 30 pC of charge were generated at a pulse duration of 1 ps. A typical application requires pulses on the order of 250 pC at 10 ps.

The conversion shown in Fig. 4 represents a typical result at a sufficient conversion efficiency. It can be seen that shape outlines are preserved. However since $E_{UV} \propto E_{IR}^4$ it is practically impossible to preserve the homogeneous filling of the volume. Distortions can then only be corrected if the correction fulfils the condition in Eq. (1).

Thus we have to conclude, that a shape preserving double conversion is impractical and the order has to be switched, such that amplified short IR pulses are first converted to VIS, stretched, shaped and then converted again. A preliminary setup without VIS stretcher and only a single shaper was able to produce significantly more homogeneous results as seen in Fig. 5.

2D + 1D PARABOLOID

For a typical European XFEL working point with a bunch charge of 250 pC, we have compared three different longitudinal electron bunch shapes with and without transverse truncation in simulations. With identical transverse size the longitudinal length has been matched such that the peak current is the same for all distributions.

The phase space is plotted in a radial density plot in Fig. 6 as introduced in [7]. First we can note that the core emittance is very similar in all cases and that a worsened emittance is largely due to a small fraction of the charge occupying a large phase space. If this charge was to be truncated, the

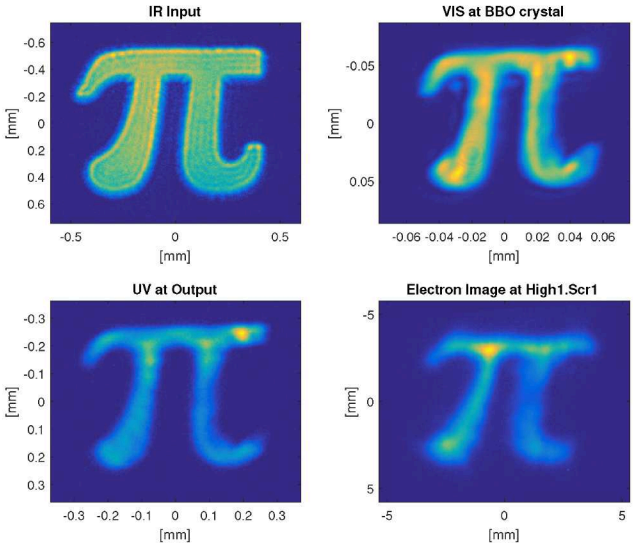

Figure 3: Transverse beam profile in **a)** IR before conversion **b)** VIS at BBO location **c)** UV at conversion section output **d)** electron beam on fluorescent screen

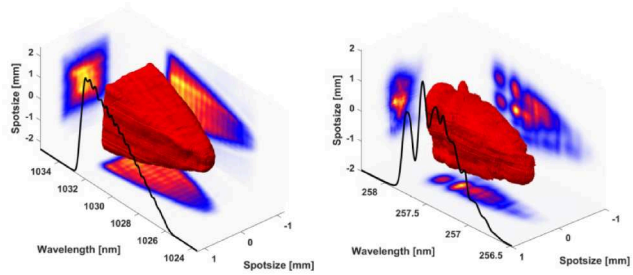

Figure 4: Spectrograph scans for triangle pulses with IR double shaper **a)** IR before conversion and **b)** after 2 consecutive conversions to UV.

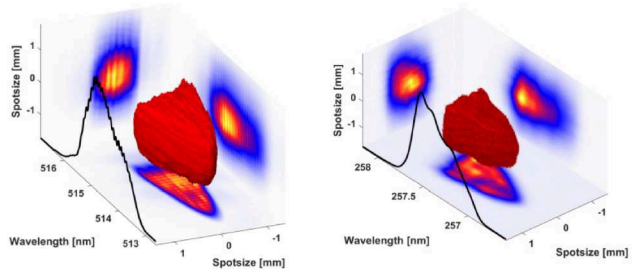

Figure 5: Spectrograph scans for triangle pulses with VIS single shaper **a)** VIS before conversion and **b)** after conversion to UV.

ISBN: 978-3-95450-220-2 ISSN: 2673-5474 doi: 10.18429/JACoW-FEL2022-WEAO4

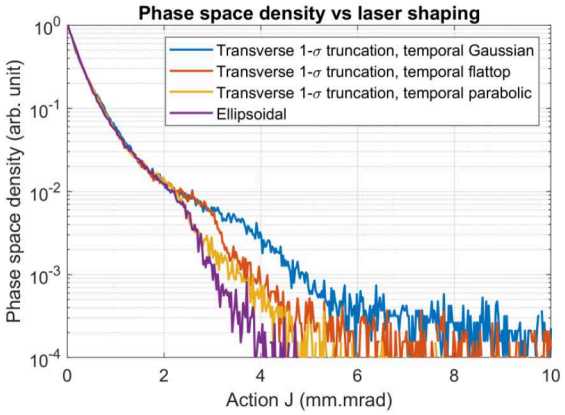

Figure 6: Radial phase space density plot for different pulse shapes and quasi parabolic transverse profiles. Emittances are summarized in Table 1

difference between the cases vanishes quickly. Since the Ellipsoidal case, which yields best performance in all cases, has a transverse parabolic projection, we compared the different longitudinal cases with the ellipsoid using flattop and quasi parabolic transverse shapes. The quasi parabolic shape is a 2D transverse Gaussian, cropped at 1 σ. Improved emittances from transverse cropping has already been experimentally proven by S. Li et. al. [8].

Table 1: Shape comparison

laser shapes	100% emit	95% emit	Action < 2 Emittance	Action < 2 percentage	core emit
Transverse Flattop					
Gauss	0.70	0.42	0.36	92.0%	0.29
Flattop	0.61	0.41	0.37	92.9%	0.28
Parabolic	0.53	0.39	0.37	93.9%	0.28
Transverse Parabolic					
Gauss	0.66	0.37	0.36	94.4%	0.30
Flattop	0.53	0.34	0.36	96.0%	0.30
Parabolic	0.43	0.33	0.37	97.5%	0.30
Ellipsoid	0.40	0.32	0.36	98%	0.29

In particular the longitudinal parabolic shape is close to the ellipsoid performance regarding the radial phase space. Hence we conclude that the most important property of the ellipsoid regarding high brightness are the parabolic projections, which do not require a spatially and temporally correlated approach and could be achieved separately with a temporal and a transverse shaper. The main ability of our 3D shaping approach is the separable control of charge and charge density along the temporal axis, which could allow to control the slice emittance mismatch in distributions like the ones needed for high transformer ratio plasma wake drivers [3]. In this application a triangular integrated charge profile is required. If the triangular profile is created with decreasing charge density, a problematic slice emittance mismatch is created, which could be avoided using transverse tapering as shown in Fig. 4.

SUMMARY

The pulse shaping method using two SLM shapers in Martinez configurations yields convincing results, given the limitations from the condition Eq. (1). The application is however severely limited by the necessity to convert the wavelength in a shape preserving way. The strength of some distortions effects, like nonlinear walkoff and NDoF, can be limited by trading off conversion efficiency. If a conversion to the fourth harmonic of the shaped wavelength is required, the high sensitivity to input intensity poses significant practical problems to preserve the shaped distributions. Ideally the shaped pulses are applied directly to a VIS sensitive photo cathode, but shape preservation could be sufficient for practical applications if only one conversion to the second harmonic is required. In order to achieve high brightness beams the authors want to point out the possibility of parabolic shaped pulses, which have a similar beam quality compared to ellipsoidal shapes. This shape can be produced with a 1D longitudinal shaper and additional 2D transverse shaper. The temporal spatial correlation approach presented, could benefit applications which require time resolved and separable tuning of charge and charge density.

REFERENCES

[1] T. Rublack *et al.*, "Production of quasi ellipsoidal laser pulses for next generation high brightness photoinjector", *Nucl. Instr. and Meth. Sect. A*, vol. 829, pp. 438–44, 2016. doi:10.1103/PhysRevAccelBeams.20.080704

[2] H. J. Qian, M. Krasilnikov, and F. Stephan, "Beam Brightness Improvement by Ellipsoidal Laser Shaping for CW Photoinjectors", in *Proc. FEL'17*, Santa Fe, NM, USA, Aug. 2017, pp. 432-435. doi:10.18429/JACoW-FEL2017-WEP008

[3] G. Loisch *et al.*, "Photocathode laser based bunch shaping for high transformer ratio plasma wakefield acceleration", *Nucl. Instr. and Meth. Sect. A*, vol. 909, pp. 107-110, 2018. doi:10.1016/j.nima.2018.02.043

[4] S. Mironov *et al.*, "Shaping of cylindrical and 3D ellipsoidal beams for electron photoinjector laser drivers", *Appl. Opt.*, vol. 55, pp. 1630-1635, 2016. doi:10.1364/AO.55.001630

[5] I. Will *et al.*, "Generation of flat-top picosecond pulses by coherent pulse stacking in a multicrystal birefringent filter", *Opt. Express*, vol. 16, pp. 14922-14937, 2008. doi:10.1364/OE.16.014922

[6] J. P. Torres *et al.*, "Angular dispersion: an enabling tool in nonlinear and quantum optics", *Adv. Opt. Photonics*, vol. 2, pp. 319–369, 2010. doi:10.1364/AOP.2.000319

[7] C. Richard *et al.*, "Measurements of a 2.1 Mev h-beam with an allison scanner", *Rev. Sci. Instrum.*, vol. 91, p. 073301, 2020. doi:10.1063/5.0004502

[8] S. Li *et al.*, "Ultraviolet laser transverse profile shaping for improving x-ray free electron laser performance", *Phys. Rev. Accel. Beams*, vol. 20 p. 080704, 2017. doi:10.1103/PhysRevAccelBeams.20.080704